RSC Advances

ROYAL SOCIETY OF CHEMISTRY

www.rsc.org/advances

Manuscript ID: RA-ART-12-2014-016564

Synthesis of vanadium pentoxide nanoneedles by physical vapour deposition and their highly sensitive behavior towards acetone at room temperature

Shah Abdul Hakim[a], Yueli Liu[a], Galina S. Zakharova[b], Wen Chen[a,*]

[a] State Key Laboratory of Advanced Technology for Materials Synthesis and Processing, and School of Materials Science and Engineering, Wuhan University of Technology, Wuhan 430070, P. R. China

[b] Institute of Solid State Chemistry, Ural Branch of the Russian Academy of Sciences, 620990 Ekaterinburg, Russian Federation

Correspondent:

[*] Prof. Wen Chen

Tel.: +86 27 8765 1107

Fax: +86 27 8776 0129

E-mail: **chenw@whut.edu.cn (Wen Chen)**

Abstract

The V_2O_5 nanoneedles were synthesized by a facile physical vapour deposition approach. XRD patterns confirm good crystallinity of the as prepared nanoneedles. Chemical states of V_2O_5 nanoneedles were confirmed through XPS analysis. Sensors based on V_2O_5 nanoneedles were investigated for four types of gases (acetone, ammonia, ethanol and propylamine) at room temperature. High reproducible response and good selective behavior towards acetone was observed in both low and high concentration zones with the low detection limit of 941 ppb, which was explained on the basis of energy band model. The sensing mechanism has also been suggested.

1. Introduction

In order to facilitate community, the increasing enactment with nanotechnology in different applications have launched a competitive research run among the material scientists, such as supercapacitors, catalysis, solar cells and chemical sensors etc. In particularly, chemical sensors have been concentrated for their distinct services including laboratories, envirmental control, food and other industries, alcohol detection and security purposes. Metal oxide nanomaterials with various kinds of morphologies have been explored for different volatile organic compounds (VOCs) detection. These multi-dimensional nanomaterials exhibit increasing number of active sites and hence execute very good sensing properties.[1] A perfect sensor must have more characteristics such as ability to detect low analyte concentration, stability for long term usage, fast response time, good selectivity in the presence of interfering analytes and a reasonable working temperature to avoid high power consumption.[2]

Among VOCs, acetone is more volatile which is often used as an organic solvent or chemical intermediate in laboratory and industries. Recently some reports disclose about certain side effects of acetone on human health whether produced by body itself (internally) or inhaled from external environment. These include irritation of eye and respiratory system, biliousness, indolence and drowsiness of nervous system on continuous exposure to acetone.[3] Further, the emission of acetone during long term storage of potatoes [4] also conveys the significance of its detection in food industries. Moreover, the need of acetone gas sensors as a breath markers to type-I diabetes is also pressing due to some certain reports.[5-7]

Various sensing materials have been explored aiming at the detection of acetone such as TiO_2 thin films[1] and nanoparticles,[8] Nb doped TiO2,[9,10] Au doped ZnO nanowires,[11] etc, however, the detection limit and working temperature were too high

to limit their application in food storage and industry, which results in huge power consumption. Selectivity is also a widely accepted issue for gas sensors, till now there are a few works focus on the high selectivity towards acetone based on the above nanomaterials.

Vanadium pentoxide (V_2O_5) is n-type transition metal oxide with interesting layered structure and electronic conductivity ~ 0.5 Scm^{-1} at room temperature.[12] It is a non-stoichiometric material which is known for its catalytic properties in oxidation reactions.[13] These properties make it well suitable for the construction of functional materials and novel devices for operation under ambient conditions. One dimensional V_2O_5 nanostructures (nanorods, nanobelts, and nanotubes etc.) have already been investigated for sensing of different gases such as ethanol, ammonia, amine and toluene.[12, 14-16] However, the major drawback with these nanostructures is their functional limitation to detect only high concentration of these gases. Acetone sensing behaviour is also not studied till now.

In this work, we report the synthesis of V_2O_5 nanoneedles by physical vapour deposition approach in a controlled atmosphere. Sensors based on V_2O_5 nanoneedles exhibit significant response to acetone at room temperature even in a very low concentration range with reasonable response time. High selectivity of the sensors and their stable response to acetone at low concentration level is explained on the basis of energy band model, and a reasonable mechanism has also been suggested.

2. Experimental

2.1 Synthesis of V_2O_5 nanoneedles

V_2O_5 nanoneedles were grown by following procedure. Si (001) substrates, polished by silicate on one side, were pre-treated by sonication in ethanol/deionized water for 10 min. After drying in a conventional oven at 80^{o}C under air, the substrates were

loaded on a quartz boat filled with 500 mg V_2O_5 powder (purity: 99%, Shanghai Shan Pu Chemical Engineering) as a raw source material and the silicate surface of the substrate faced down towards the source powders at a vertical distance of 5 mm. The quartz boat was then inserted inside a glass tube (one meter in length) exactly at the mid-point, which was placed inside a horizontal tube furnace under air and sealed tightly. Temperature was increased to 450 ^oC (growth temperature) at the rate of 10^oC/min under air and subsequently from 450 to 650^oC at the rate of 0.5^oC/min to stabilize the growth. At this stage, Ar gas was allowed to inject in at the flow rate of 0.2 L/min and the heating was continued to 710 ^oC beyond the melting point of V_2O_5 (~690 ^oC) at the rate of 3C^o/min. Quartz tube was maintained at 710 ^oC for 40 min under Ar flow of 0.1L/min and was finally cooled to room temperature such that the flow of Ar gas was stopped at the demoted temperature value of 690 ^oC. It was noted that after deposition, silicate surface of the substrates turned as yellowish.

2.2 Characterization

The deposited nanoneedles products were then characterized by X-rays diffractometer (XRD, D/MAX-III, Cu Kα) and high magnification scanning electron microscopy (SEM, Zeiss Ultra Plus, ZEISS, Germany) for investigation of structure and morphology, respectively. X-ray photoelectron spectroscopy (XPS) measurement was performed in the Escalabmk-Ⅱ XPS apparatus (VG Scientific, England) with Al target. The emission angle between the photoelectron beam and the sample surface was 45°, and the calibration of the binding energy of the electron spectrometer was made by using the maximum adventitious C1s signal at 284.6 eV with the solution of the full width at half maximum (FWHM) being 0.8 eV.

2.3 Fabrication and measurement of gas sensor

For gas sensing measurements, the deposited V_2O_5 nanoneedles were scrapped off the substrates surface in following manner. Substrates with grown V_2O_5 nanoneedles were heated at 60^{o}C under air, followed by sonicating in ethanol for 30 mins. Ethanol was evaporated and nanoneedles were mixed with terpineol to obtain a smooth paste. The paste was then coated on the surface of a ceramic tube, on which a pair of Au electrode was already printed. These devices were dried at 100 ^{o}C for 3 days in air to decompose terpineol completely. Finally, a Ni-Cr heating wire was inserted into the tube. Before testing the gas sensing properties, the fabricated V_2O_5 nanoneedles sensor was aged at 60 °C for 5 days to improve the stability of the sensitive materials.

The gas sensing properties were tested on a WS-30A measuring system containing static gas distribution chamber with a volume of 18 litres. During the testing process, the gas sensors were placed in the centre of the test chamber, in series connection with an external resistor name as RL. In the gas testing process, liquid vaporization method was used to produce target gas with certain concentration. Typically, certain amount of liquid was injected into a heater base fitted inside the test chamber by means of micro-syringe. When heated, the liquid got volatilized into concerned test gas, which forms a simulation environment of the indoor air with gaseous vapours. Four types of liquid analytes (Acetone, ammonia, ethanol and propylamine) were taken for tests at room temperature. Relation between volume of the injected liquid and concerned gas concentration can be derived from a general formula,[17] and is written as,

$$\mathbf{Q} = \left(\frac{\mathbf{7.85x10^{-10}\,M}}{\mathbf{d.p}}\right)\mathbf{C} \qquad \mathbf{(1)}$$

Where Q denotes the injected liquid volume in µl, M is the molar mass of test gas, d is the liquid density, p is the concerned liquid concentration and C is the gaseous

concentration in ppm. The response was defined as the ratio of the resistance in air (R_a) to that in target gas (R_g), namely $S = R_a/R_g$.

3. Results and discussion

The XRD pattern of as-prepared sample is shown in **Fig. 1(a)** and the diffraction peaks are indexed to orthorhombic V_2O_5 (JPCDS 01-086-2248). Besides, two peaks at $2\theta = 10.60^o$ and 12.20^o also appear in the pattern which are related to (021) and (211) planes of SiO_2 phase of Si substrate and no other impurities are observed which indicates the good crystallization degree of V_2O_5 nanoneedles.

SEM images in different magnifications of the V_2O_5 products are shown in **Fig. 1(b-d)**. The low magnification image **(Fig. 1(b))** reveals the uniform growth of V_2O_5 nanoneedles on Si substrates. In order to obtain further clear insight into the microstructure, high magnification images are displayed in **Fig. 1(c, d)**. It can be seen that each nanoneedle consists of wide base and a sharp tip. Typical diameters of the base part and sharp tip are in the range of 30-40 nm and 11-15 nm, respectively, and the length of nanoneedle is 100-200 nm. Such a conical shaped nanoneedle might be effective for better gas adsorption and electron transport during interaction with the analyte molecules because they form disordered chains in the form of zigzag geometry when they are randomly oriented over ceramic tube in gas sensing device. Such a network of nanoneedle is responsible for frequent gas adsorption.[18-20]

Fig. 1(e, f) displays TEM and HRTEM images of V_2O_5 nanoneedles with the corresponding SAED pattern (inset). The image clearly indicate the preferential growth of the nanoneedles along (010) plane, which has significant effect in analyte-surface adsorption.[21] The effect will be discussed in detail in the sensing mechanism part.

X-ray photoelectron spectroscopy (XPS) data for V_2O_5 nanoneedles sample is shown in **Fig. 2**. Survey spectrum in **Fig. 2(a)** indicates the appearance of Si2p, C1s, V2p and O1s peaks. Si2p peak appears as the nanoneedles were deposited on Si substrate and C-1s peak appears due to electrodes during the test. **Fig. 2(b)** displays the fitted profile of vanadium peaks, which shows that V $2p^{3/2}$ peak appears at binding energy 517 eV, related to V^{5+} state of V_2O_5 phase.[22-25] Si (2p) appears at the binding energy 103.53 eV and corresponds to Si^{4+} state of SiO_2 surface of Si substrate and is shown in **Fig. 2(c).** The oxygen peaks lie at three binding energies 530.47 eV, 532.52 eV and 533.55 eV, related to 1s state of oxygen for V_2O_5, SiO_2 and adsorbed oxygen ions, respectively **(Fig. 2(d))**.[26,27]

The resistance change of V_2O_5 nanoneedle sensors towards acetone was measured as shown in **Fig. 3(a)**, in which variation of resistance in steady state mode is plotted. Acetone was injected in two concentration zones, the low concentration zone is comprised of range from 863 ppb to 4.3 ppm and high concentration zone ranges from 8.63 ppm to 140 ppm. Resistance of the V_2O_5 nanoneedle sensors decreases upon the injection of acetone gas and reaches its baseline value when the gas is released. Decline in resistance amplifies with the increasing acetone concentration, and this is the characteristic of n-type V_2O_5 sensor. Corresponding sensitivity response is shown in **Fig. 3(b)**, the sensitivity for 1.7 ppm acetone is low (S=1.025) and it increases monotonically in low concentration zone. A sharp upturn in sensitivity is noticed after the injection of acetone in high concentration zone, which obviously proves the significance of the sensor for higher concentrations and useful in food industry, particularly to protect the mass spoilage of potatoes at room temperature.[4]

Fig. 3(c, d) describe the variation of sensitivity response with acetone concentration and it is noted that the rise in sensitivity with concentration follows

almost similar curvature pattern in both low and high concentration zones, which shows its credibility of being feasible for higher concentrations beyond the selected zones by symmetry. The detection limit for acetone is estimated to be 941 ppb by using equation **(2)**,

$$DL = KS_o/m \qquad \textbf{(2)}$$

Where K is signal to noise ratio and it is a numerical factor chosen according to the desired confidence level and generally equal to 3. S_o is the standard deviation of the blank measurements (n = 120) and m is the slope of the response versus concentration curve throughout the range of concentrations.[28]

Real value response behaviour of the sensor was also studied to estimate the response times for the extreme low concentration (1.7 ppm) **(Fig. 4(a))**. Response time of 73s is noted, which decreases slightly with the increase in concentration till it verges on 67s for 140 ppm **Fig. 4(b)**. After releasing the gas, sensor resistance recovers fast to base-line state. Variation of response time with acetone concentration in both low and high zones is plotted in **Fig. 4(c, d)**, which shows a minute fall in response time with increasing acetone concentrations in both the zones, thus representing the steadier response behaviour of the sensor.

The reproducibility of the gas response was investigated by switching the acetone gas on and off at the detection threshold level (1.7 ppm). **Fig. 5** shows the repetitive response of the V_2O_5 nanoneedle sensor to acetone at room temperature. Based on the results of four repeated steps of acetone gas modulation, the reproducibility of the V_2O_5 acetone gas sensor is observed by calculating the coefficient of variation (CV), the value is found to be 0.0211 (2.11%) as defined by $CV = \sigma/\mu$, where σ is the standard deviation and μ is the mean.[29] This observation indicates that V_2O_5 nanoneedles have stable and good sensing characteristics for acetone gas. It also

shows that such sensors have good recovery to the base-line with some signal distortion.

To predict the selectivity, steady state response of the sensor based on V_2O_5 nanoneedles was obtained in accordance with the changing concentration of gases (acetone, ammonia, ethanol and propylamine) at the room temperature. Sensor could not respond to gases other than acetone in the low concentration zone, which implies that it is perfectly selective at low concentrations. In high concentration zone (8.63-140 ppm), the sensors detect all the four gases, however, the response is more prominent to acetone such that higher sensitivity (~2.37 for 140 ppm) to acetone vapours was achieved **(Fig. 6(a))**. The real value resistance variation is obtained by subjecting the sensor to a continuous exposure/injection to air/gases alternatively, and leads to the real value response times of 67s, 49s, 34s and 88s towards 140 ppm of acetone, ethanol, ammonia and propylamine, respectively **(Fig. 6(b))**. Selectivity of the V_2O_5 nanoneedle sensor in high concentration zone is evaluated by % response magnitudes corresponding to 200 ppm of acetone, ammonia, ethanol and propylamine, which turnout to be 248%, 162%, 142% and 135%, respectively **(Fig. 6(c))**. This obviously predicts the acetone selective nature of V_2O_5 nanoneedles in high concentration zone as well. Comparison of response properties of sensors based on V_2O_5 in this work other kinds of V_2O_5 nanostructures reported earlier is described in **Table 1.**

Sensing mechanism of sensors based on V_2O_5 nanoneedle sensor may be explained on the basis of energy band model.[17] We know that V_2O_5 is n-type semiconductor with intrinsic defects due to stoichiometric deviation in its crystal, such as oxygen vacancies.

Quantitatively, conductivity change is governed by E_g value which is defined as $E_g = E_c - E_v$ for n-type semiconductors and can be derived as following.

Carrier density in semiconductors is expressed as,

$$n_o(p_o) = \frac{2\left(2\pi m^*_{n(p)} K_B T\right)^{3/2}}{h^3} \exp\left[\mp\left(\frac{E_{cv}-E_f}{K_B T}\right)\right] \qquad (3)$$

Where n_o and p_o represent electron and holes densities, which are majority charge carriers for n-type and p-type semiconductors, respectively. $m^*_{n(p)}$ is the effective masses of electrons/holes. K_B and h are Boltzmann and Plank's constants. E_f represents fermi level and E_{cv} is the highest band which is conduction band for n-type and valance band for p-type semiconductors and here we consider it as E_c of the conduction band.[31] The conductance (conductivity) is directly proportional to the carrier concentration, which is equal to $n_o p_o$ and can be written as,

$$n_o p_o = 4\left(\frac{2\pi K_B T}{h^2}\right)^3 \left(m^*_n . m^*_p\right)^{3/2} \exp\left[-\left(\frac{E_g}{K_B T}\right)\right] \qquad (4)$$

Under certain temperature, m^*_n and m^*_p are constants, so the conductivity is mainly controlled by the exponential term (exp ($-E_g/k_B t$)) or simply by E_g value, which is related with the adsorption of analyte molecules to the sensor surface in following manner.

Adsorption of analyte (acetone) molecules on the V_2O_5 nanoneedle surface occurs in two steps including physical adsorption and chemical adsorption. Oxygen molecules from air are physically adsorbed on nanoneedle surface and trap electrons there to form chemically adsorbed oxygen ions through following reaction.

$$O_{2(ads)} + e^- \longrightarrow O_2^- \qquad (5)$$

Such kind of adsorption of molecular oxygen ion is confirmed from linear fit of $\log (S_g - 1) = \log C$ **(Fig. 6(d))**. Slopes of linear fit equations corresponding to acetone, ethanol, ammonia and propylamine turn out to be 0.32, 0.34, 0.45 and 0.37,

respectively, which are closer to 0.5 (typical value for oxide ion adsorption),[32,33] and therefore predict adsorption of such ions on nanoneedle surface at room temperature. However this is an exothermic reaction and chemisorption rate is slow at room temperature,[14] which is the phenomenological reason for the relatively low value of sensitivity of nanoneedle sensor. These oxygen ions distribute themselves on V_2O_5 surface in the form of VO surface groups, which are responsible for catalytic oxidation of hydrocarbons. In V_2O_5, the VO groups are located on (010) plane because this surface is the lowest free energy surface in V_2O_5.[21] This produces electron depletion region of high electric potential (qV_s) due to high baseline resistance of the sensor.

After the injection of analyte (e.g. acetone), its molecules are chemisorbed on V_2O_5 surface. The acetone molecule tends to be adsorbed on the stable and lowest free energy surface (010) of V_2O_5 lattice, which is shown schematically in **Fig. 7.** The reducing acetone molecule will react with chemisorbed oxygen ion O_2^- and liberate the trapped electron back to V_2O_5 surface. Ideal chemical reaction is as following.

$$(CH_3)_2CO + 4\,O_2^- \longrightarrow 3CO_2 + 3H_2O + 4e^- \qquad \textbf{(6)}$$

Detailed oxidation mechanism of acetone involves the formation of intermediate products acetate and formaldehyde on the V_2O_5 surface, and then ultimately produces the final product CO_2.[34] Acetate reactis with hydrogen atom to form a nearby hydroxyl group and stabilizes to acetic acid. This step is exothermic by 0.6 Kcal/mol. Similarly the oxidation of intermediate formaldehyde over (010) surface of V_2O_5 is also exothermic by 22.1 Kcal/mol.[35] Besides, the final reaction involving the production of CO_2 is exothermic by 30 kcal/mol. Such exothermic reactions are responsible for self-evaporation of H_2O which is the final by-product in acetone oxidation. However, in order to avoid its effect on the stability of the sensor surface,

extreme care was taken during recording the gas sensing measurements e.g. prior to subsequent measurements, a little bit heat treatment was given to the sensor, followed by a certain time delay for turning the sensor surface cool down to room temperature.

The oxidation reaction leads to lowering of qV_s value and hence reduces the electron depletion layer, which further decreases the resistance of V_2O_5. The adsorption leads to charge transfer from acetone molecule to V_2O_5 nanoneedle surface through chemisorbed oxygen ion medium and adsorption induced reconstruction of V_2O_5 surface. These two mechanisms are responsible for surface charge distribution on V_2O_5 nanoneedle and therefore changing in energy band gap E_g is observed, which produces change in conductance of the sensor.

Higher acetone selective nature of V_2O_5 nanoneedle sensor than other analytes may be explained on the basis of chemical reactivity of reducing gas molecules at the sensor's surface. Acetone contains the carbonyl functional group. Due to greater electronegativity of oxygen, carbonyl group is a polar functional group and therefore acetone has larger dipole moment (D=2.88).[36] Oxygen atom in carbonyl group of acetone has higher electron density due to lone pairs than the carbon atom. Acetone's reactivity may be rationalized taking into account the important resonance contributor comprising of a positive carbon and negative oxygen. Polarity of the group has a profound effect on the chemical reactivity of acetone. The most energetically favourable reaction channel is that a surface oxygen atom attacks the carbonyl carbon to form a C-O bond with a bond length of 1.58 Å during the oxidation of acetone, while the activated C-C bond is elongated to 1.93 Å. By overcoming an energy barrier of 31.5 kcal/mol, the breaking of the C-C bond leads to an acetic group, CH_3COO*(acetic acid), and a formaldehyde molecule (O* denotes the lattice oxygen) on the surface. Such a favourable deep oxidation of acetone over V_2O_5 (010) surface

plane has already been confirmed by periodic DFT method,[35, 37] which shows a good selective nature of gas sensors based on V_2O_5 surface.

4. Conclusions

V_2O_5 nanoneedles were synthesized through an effective physical vapour deposition method. Sensors based on V_2O_5 nanoneedles exhibit significant sensing properties towards acetone compared to ammonia, ethanol and propylamine at room temperature with almost steady response time, particularly in the high detection zone (8.63-140 ppm). The tremendous sensing properties have been explained qualitatively as well as quantitatively, which infers its potential application for practical purposes specifically in food industries. A suitable sensing mechanism has also been suggested for V_2O_5 nanoneedles sensors.

Acknowledgements

This work is supported by the International S&T Cooperation program of China (ISTCP) (No. 2013DFR50710), Equipment pre-research project (No. 625010402), Science and Technology Support Program of Hubei Province (No. 2014BAA096), the National Nature Science Foundation of Hubei Province (No. 2014CFB165), and Ministry of Education and Science of Russia (No. 14.613.21.0002).

References

1. S. Capone, A. Forleo, L. Francioso, R. Rella, P. Siciliano, J. Spadavecchia, D. S. Presicce and A. M. Taurino, *J. Optoelectron. Adv. Mater.*, 2003, **5**, 1335.
2. Z. Liu, T. Yamazaki, Y. Shen, T. Kikuta, N. Nakatani and T. Kawabata, *Appl. Phys. Lett.*, 2007, **90**, 1731191.
3. B. Bhowmik, K. Dutta, A. Hazra and P. Bhattacharyya, *Solid-State Electron.*, 2014, **99,** 84.
4. B. P. Costello, R. J. Ewen, H. E. Gunson, N. M. Ratcliffe and P. T. Phillips, *Meas. Sci. Technol.*, 2000, **11**, 1685.
5. A. M. Diskin, P. Spanel and D. Smith, *Physiol. Meas.,* 2003, **24**, 107.
6. C. H. Deng, J. Zhang, X.F. Yu, W. Zhang and X. M. Zhang, *J. Chromatogr. B,* 2004, **810**, 269.
7. M. Righettoni, A. Tricoli, and S. E. Pratsinis, *Anal. Chem.,* 2010, **82***,* 3581.
8. A. Teleki, S. E. Pratsinis, K. Kalyanasundaram and P. I. Gouma, *Sens. Actuators, B*, 2006, **119**, 683.
9. V. Galstyan, E. Comini, G. Faglia, A. Vomiero, L. Borgese, E. Bontempi and G. Sberveglieri, *Nanotechnology*, 2012, **23**, 2357061.
10. S. Phanichphant, C. Liewhiran, K. Wetchakun, A. Wisitsoraat and A. Tuantranont, *Sensors*, 2011, **11**, 472.
11. S. J. Chang, T. J. Hsueh, I. C. Chen, S. F. Hsieh, S. P. Chang, C. L. Hsu, Y. R. Lin and B. R. Huang, *IEEE Trans. Nanotechnol.,* 2008, **7**, 754.
12. A. D. Raj, T. Pazhanivel, P. S. Kumar, D. Mangalaraj, D. Nataraj and N. Ponpandian, *Curr. Appl. Phys.,* 2010, **10**, 531.
13. C. V. Ramana, O. M. Hussain, N. B. Srinivasalu, C. Julien and M. Balkanski, *Mater. Sci. Eng., B*, 1998, **52**, 32.

14. J. Liu, X. Wang, Q. Peng and Y. D. Li, *Adv. Mater.*, 2005, **17**, 764.

15. I. Raible, M. Burghard, U. Schlecht, A. Yasuda and T. Vossmeyer, *Sens. Actuators, B*, 2005, **106**, 730.

16. S. A Hakim, Y. Liu, Y. Lu and W. Chen, *Mater. Sci. Semicond. Process.,* 2015, **31**, 630.

17. W. Tang and J. Wang, *Sens. Actuators, B*, 2015, **207**, 66.

18. F. K. Butt, C. Cao, W. S. Khan, M. Safdar, X. Fu, M. Tahir, F. Idrees, Z. Ali, G. Nabi and D. Yu, *CrystEngComm.*, 2013, **15**, 2106.

19. F. Nieto, A. A. Tarasenko, C. Uebing and V. Pereyra, *Langmuir*, 1999, **15**, 5893.

20. J. Arbiol, E. Comini, G. Faglia, G. Sberveglieri and J. R. Morante, *J. Cryst. Growth*, 2008, **310**, 253.

21. A. Andersson, *J. Solid State Chem.*, 1982, **42**, 263.

22. W. E. Slink and P. B. Degroot, *J. Catal.*, 1981, **68**, 423.

23. J. Kasperkiewicz, J. A. Kovacich and D. Lichtman, *J. Electron. Spectrosc. Relat. Phenom.*, 1983, **32**, 123.

24. M. K. Takagi, M. Soma, T. Onishi and K. Tamaru, *Can. J. Chem.,* 1980, **58**, 2132.

25. H. J. Choi, J. S. Kim and M. Kang, *Bull. Korean. Chem. Soc*., 2007, **28**, 581.

26. R. Gopalakrishnan, B. V. R. Chowdari and K. L. Tan, *Solid-State Ionics*, 1992, **53**, 1168.

27. M. L. Miller and R. W. Linton, *Anal. Chem.,* 1985, **57**, 2314.

28. L. Yang, H. Lin, Z. Zhang, L. Cheng, S. Ye and M. Shao, *Sens. Actuators, B,* 2013, **177**, 260.

29. H. H. Park, N. J. Choi, H. Kang, M. Y. Jung, J. W. park, K. H. Park and D. S. Lee, *Sens. Actuators, B,* 2014, **203**, 282.

30. W. Jin, B. T. Dong, W. Chen, C. X. Zhao, L. Q. Mai and Y. Dai, *Sens. Actuators, B*, 2010, **145**, 211.

31. E. K. Liu, B. S. Zhu and J. S. Luo, Semiconductor Physics, *Publishing House of Electronics Industry*, *Beijing,* 2008.

32. R. W. J. Scott, S. M. Yang, G. Chabanis, N. Coombs, D. E. Willams and G. A. Ozin, *Adv. Mater.,* 2001, **13**, 1468.

33. D. E. Williams, *Sens. Actuators, B,* 1999, **57**, 1.

34. P. P. Sahay, *J. Mater. Sci.*, 2005, **40**, 4383.

35. G. L. Dai, Z. H. Li, J. Lu, W. N. Wang, and K. N. Fan*, J. Phys. Chem. C,* 2012, **116**, 807**.**

36. O. Dorosh and Z. Kisiel, *Acta Phys. Pol., A*, 2007, **112**, S95.

37. M. Lin, T. B. Desai, F. W. Kaiser and P. D. Klugherz, *Catal. Today,* 2000, **61**, 223.

Table and Figures captions

Table 1 Comparison of sensing properties of V_2O_5 nanoneedles synthesized in this work with other V_2O_5 nanostructures reported in literature.

Figure 1 (a) XRD pattern of V_2O_5 nanoneedles deposited on Si substrates, (b) low magnification and (c, d) high magnification SEM images of V_2O_5 nanoneedles, (e) TEM image and **(f)** HRTEM image of V_2O_5 nanoneedle with surface details (SAED pattern of HRTEM image inset)

Figure 2 XPS spectrum of V_2O_5 nanoneedles deposited on SiO_2 substrate (a) survey spectrum, (b) vanadium $2p^{3/2}$ peak, (c) silicon 2p peak, (d) oxygen 1s peaks

Figure 3 (a) Steady state resistance transient time curve of sensor based V_2O_5 nanoneedle to acetone at room temperature, (b) sensitivity response versus time for different acetone concentrations, (c) variation of % sensitivity response with acetone concentration in low zone, (c) high zone

Figure 4 (a) Real value response curve of V_2O_5 nanoneedle sensor towards 1.7 ppm acetone for response time, (b) real value response curves of V_2O_5 nanoneedle sensor towards 140 ppm of various gases for response times, (c, d) variation behavior of response time in low and high concentration zones, respectively**.**

Figure 5 Repeated response curve of V_2O_5 nanoneedle sensor towards 1.7 ppm acetone over four repeated cycles of exposure

Figure 6 Fig. 6 (a) Steady state response curves of V_2O_5 nanoneedle sensors to acetone, ethanol, ammonia and propylamine in high concentration zone, (b) real value resistance continuum to all gases in dynamic mode, (c) selectivity in high concentration zone, (d) linear fit calculation for estimating oxygen ion adsorption

Figure 7 Schematic sensing mechanism of V_2O_5 nanoneedles towards acetone

Table 1 Comparison of sensing properties of V_2O_5 nanoneedles synthesized in this work with other V_2O_5 nanostructures reported in literature**.**

Material	Detection threshold (ppm)	Magnitude of sensitivity	Operating temperature (^oC)	Selectivity	Refeence
V_2O_5 nanoneedles	1.7	2.37 for 140 ppm	RT*	Acetone	**This work**
V_2O_5 nanorods	100	1.04 for 500 ppm	RT*	Ethanol	[12]
V_2O_5 nanobelts	5	3 at 1000 ppm	200	Ethanol	[14]
V_2O_5 nanotubes	-	1.8 at 1000 ppm	230	Ethanol	[30]
Fe_2O_3 activated V_2O_5 nanotubes	10	2.1 at 1000 ppm	230	Ethanol	[30]

*** RT, Room Temperature**

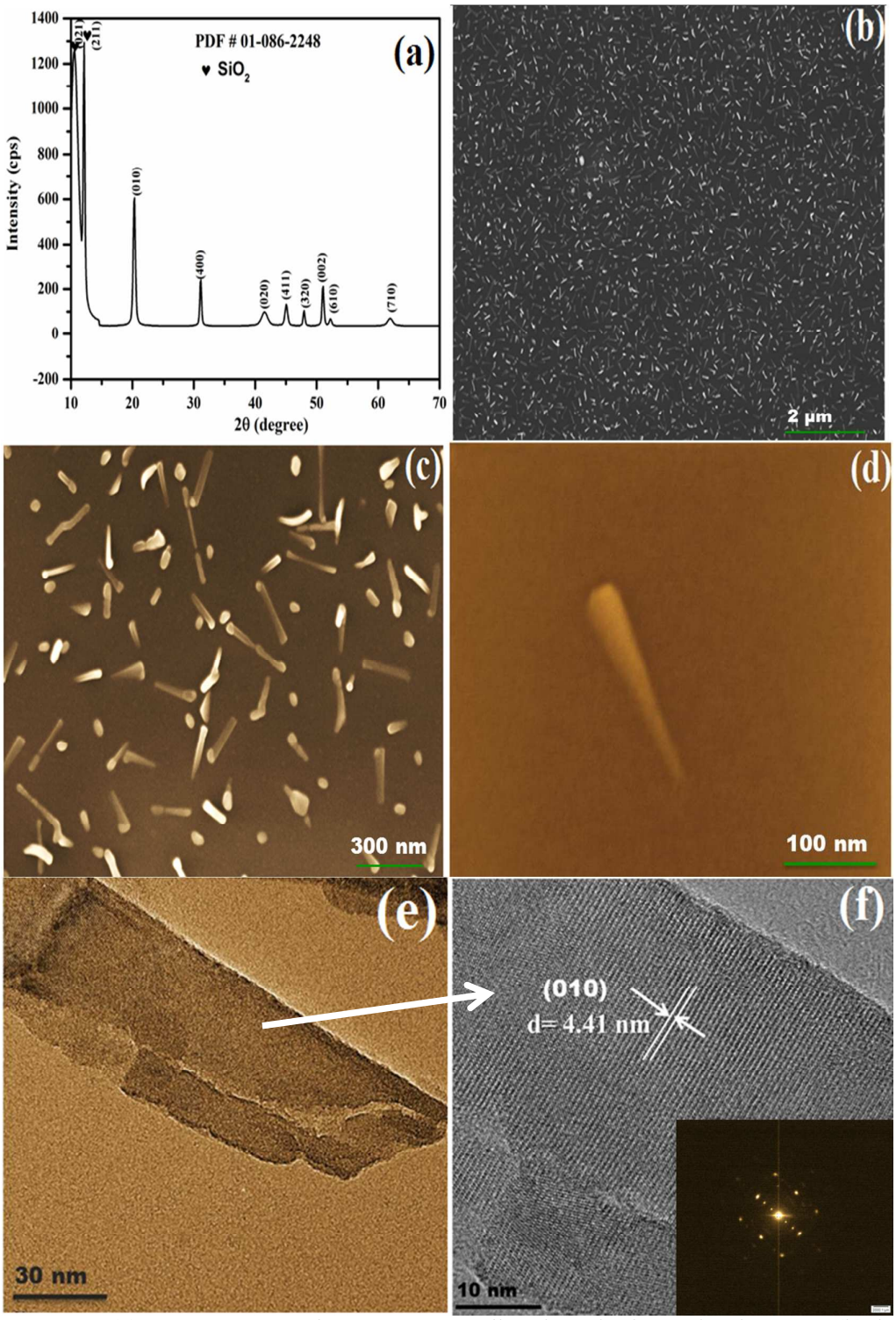

Figure 1 (a) XRD pattern of V_2O_5 nanoneedles deposited on Si substrates, (b) low magnification and (c, d) high magnification SEM images of V_2O_5 nanoneedles, (e) TEM image and **(f)** HRTEM image of V_2O_5 nanoneedle with surface details (SAED pattern of HRTEM image inset)

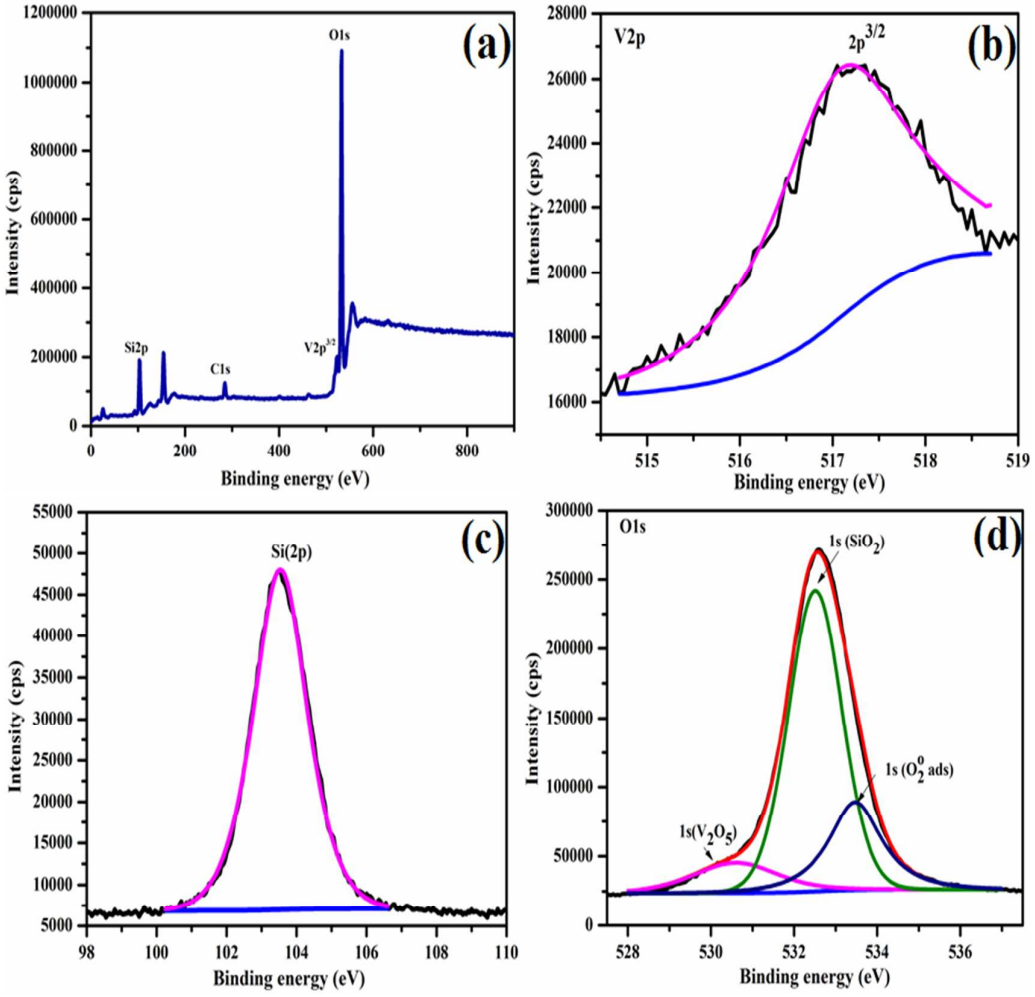

Fig. 2 XPS spectrum of V_2O_5 nanoneedles deposited on SiO_2 substrate **(a)** survey spectrum, **(b)** vanadium $2p^{3/2}$ peak, **(c)** silicon 2p peak, **(d)** oxygen 1s peaks

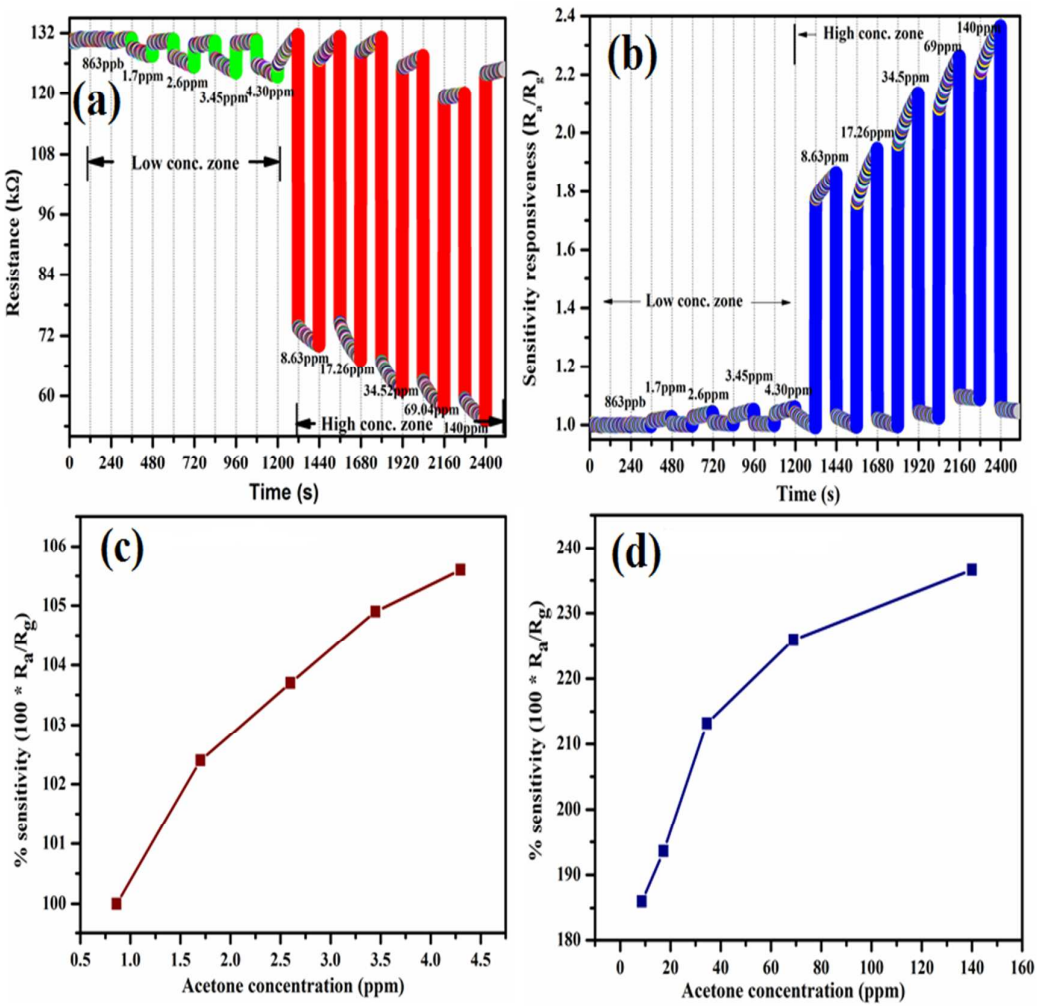

Fig. 3 (a) Steady state resistance transient time curve of sensor based V_2O_5 nanoneedle to acetone at room temperature, **(b)** sensitivity response versus time for different acetone concentrations, **(c)** variation of % sensitivity response with acetone concentration in low zone, **(d)** high zone

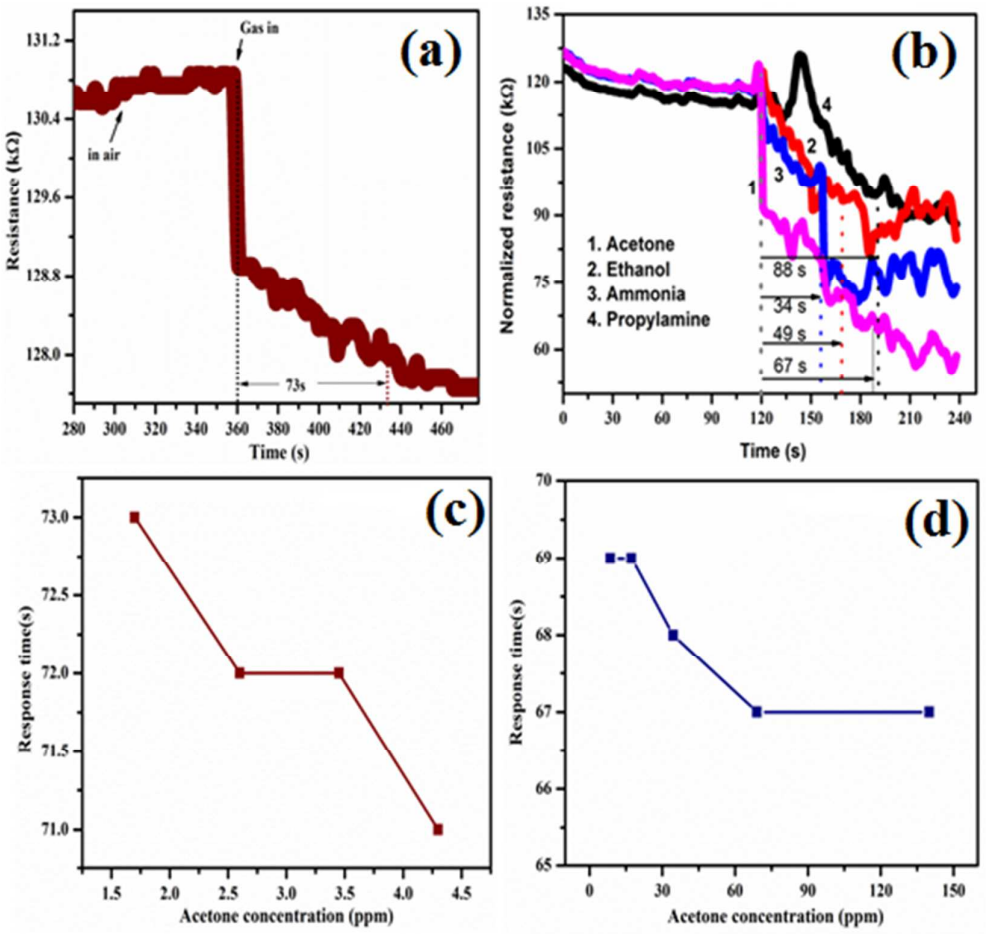

Fig. 4 (a) Real value response curve of V_2O_5 nanoneedle sensor towards 1.7 ppm acetone for response time, **(b)** real value response curves of V_2O_5 nanoneedle sensor towards 140 ppm of various gases for response times, **(c, d)** variation behavior of response time in low and high concentration zones, respectively.

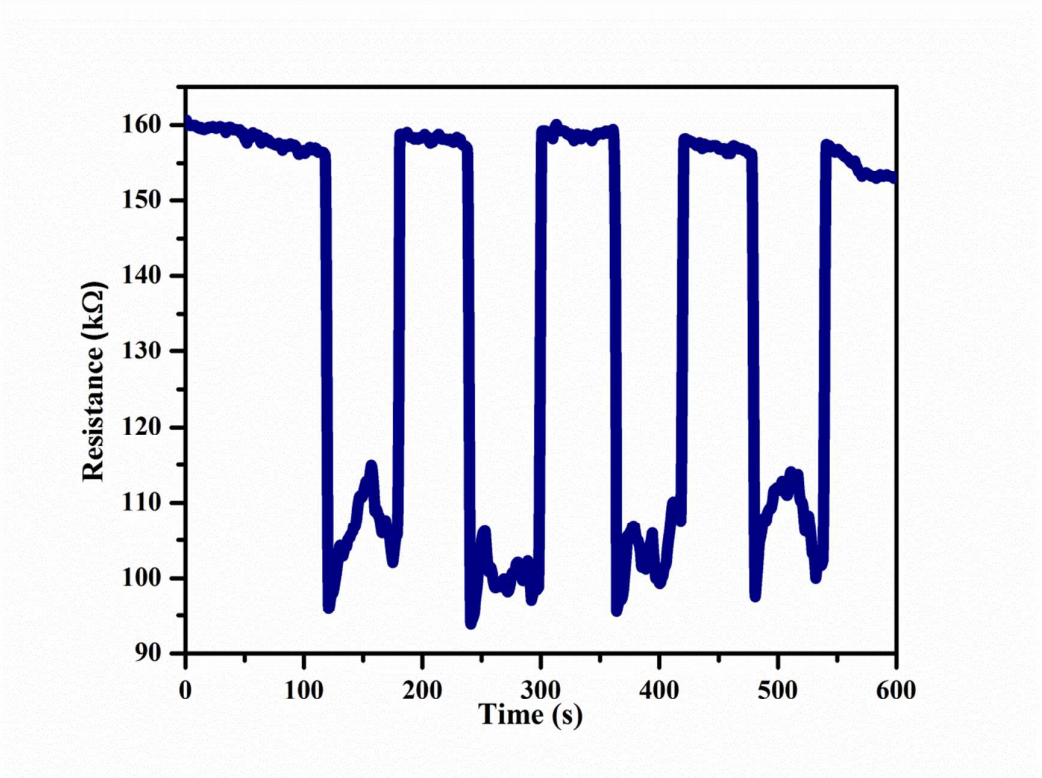

Fig. 5 Repeated response curve of V_2O_5 nanoneedle sensor towards 1.7 ppm acetone over four repeated cycles of exposure

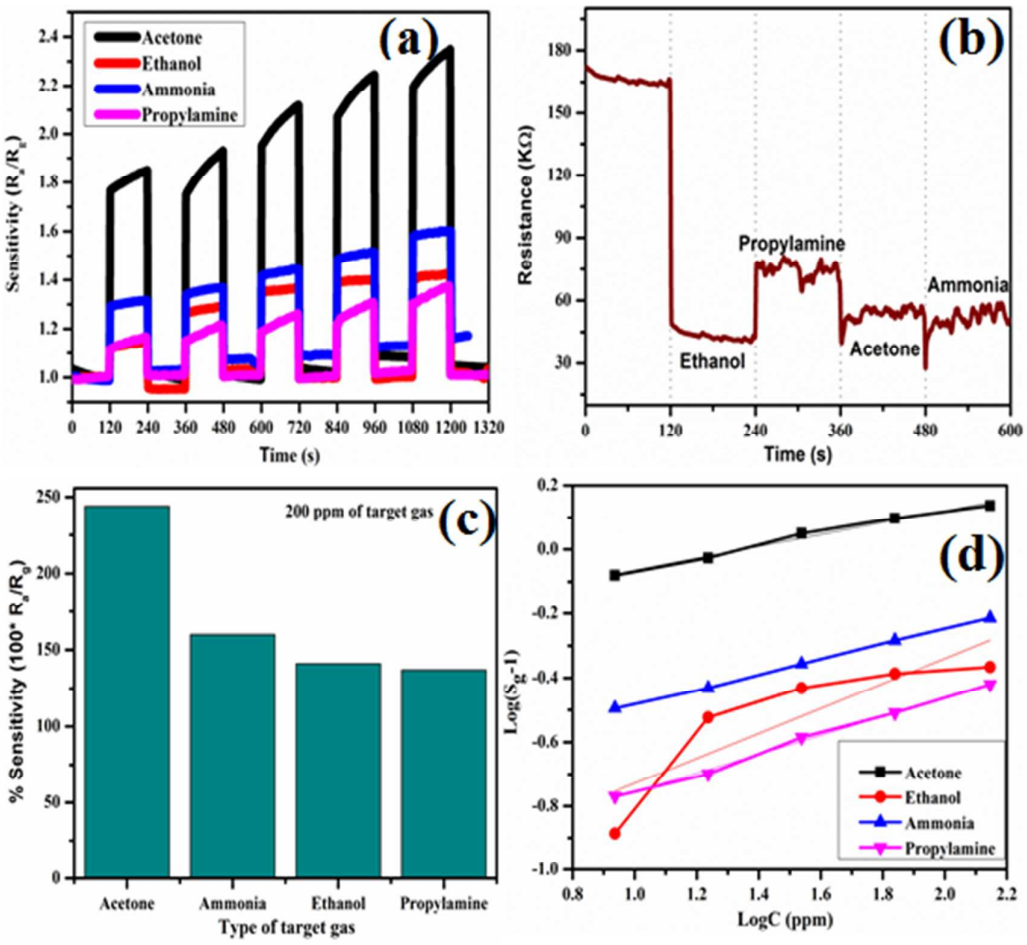

Fig. 6 (a) Steady state response curves of V_2O_5 nanoneedle sensors to acetone, ethanol, ammonia and propylamine in high concentration zone, **(b)** real value resistance continuum to all gases in dynamic mode, **(c)** selectivity in high concentration zone, **(d)** linear fit calculation for estimating oxygen ion adsorption

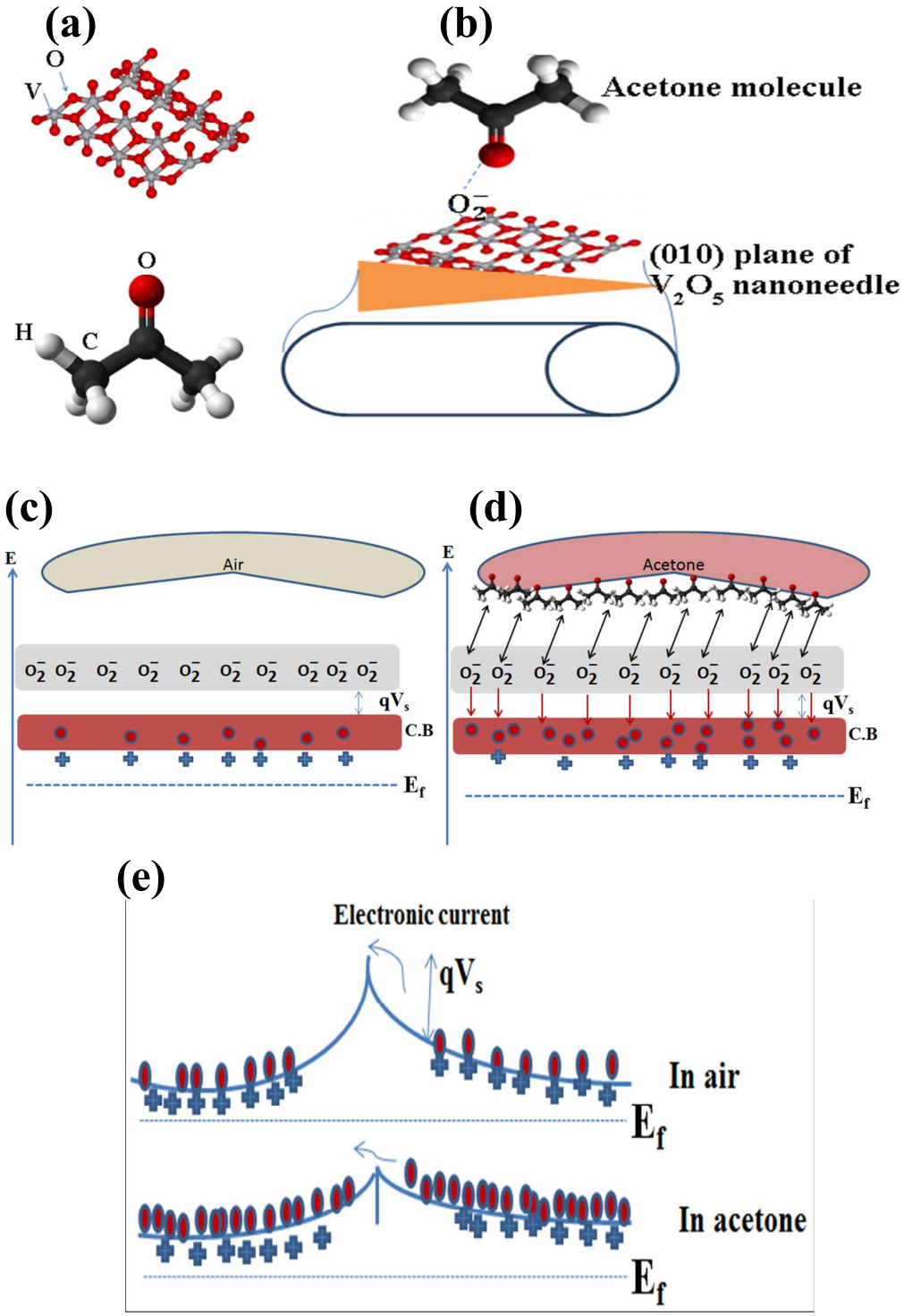

Fig. 7 Schematic sensing mechanism of V_2O_5 nanoneedles towards acetone